Published in final edited form as:
Plant J. 2014 February ; 77(3): 443–453. doi:10.1111/tpj.12361.

Direct isolation of flavonoids from plants using ultra-small anatase TiO_2 nanoparticles

Jasmina Kurepa[1], **Ryo Nakabayashi**[3], **Tatjana Paunesku**[2], **Makoto Suzuki**[3], **Kazuki Saito**[3,4], **Gayle E. Woloschak**[2], and **Jan A. Smalle**[1,*]

[1]Plant Physiology, Biochemistry, Molecular Biology Program, Department of Plant and Soil Sciences, College of Agriculture, University of Kentucky, Lexington, Kentucky 40546, USA

[2]Department of Radiation Oncology, Feinberg School of Medicine, Northwestern University, Chicago, IL 60611

[3]RIKEN Center for Sustainable Resource Science, Tsurumi-ku, Yokohama 230-0045, Japan

[4]Graduate School of Pharmaceutical Sciences, Chiba University, Inohana 1-8-1, Chuo-ku Chiba 260-8675, Japan

Summary

Surface functionalization of nanoparticles has become an important tool for the *in vivo* delivery of bioactive agents to their target sites. Here we describe the reverse strategy, nanoharvesting, in which nanoparticles are used as a tool to isolate and enrich bioactive compounds from living cells. Anatase TiO_2 nanoparticles smaller than 20 nm form strong bonds with molecules carrying enediol and especially catechol groups. We show that these nanoparticles can enter plant cells, conjugate enediol and catechol group-rich flavonoids *in situ*, and exit plant cells as flavonoid-nanoparticle conjugates. The source plant tissues remain viable after treatment. As predicted by the surface chemistry of anatase TiO_2 nanoparticles, the quercetin-based flavonoids were enriched amongst the nanoharvested flavonoid species. Nanoharvesting eliminates the use of organic solvents, allows spectral identification of the isolated compounds, and offers a new avenue for the use of nanomaterials for the coupled isolation and testing of bioactive properties of plant-made compounds.

Keywords

anatase TiO_2 nanoparticles; flavonoids; catechols; *Arabidopsis thaliana*; stress

Introduction

In recent years, studies of the interaction between nanoparticles and plants have focused on three main areas. Most of the current studies analyzed the effect of nanomaterials and, in particular, nanoparticles, on plant growth and development. These studies describe the properties of nanoparticles that influence their uptake by plants as well as their distribution in plant tissues and effects on plant physiological or biochemical processes (Navarro *et al.* 2008; Monica and Cremonini 2009; Ma *et al.* 2010; Dietz and Herth 2011; Rico *et al.* 2011; Remédios *et al.* 2012). Although the number of systematic studies in this research area is still small and prohibits any general conclusions, the current data strongly suggest that the interaction of nanoparticles with plants affects both interactors and that the effects on plants

*Corresponding author: Jan A. Smalle, 1401 University Drive, Lexington, KY 40546, USA, Phone: +1 (859) 257-3677, Fax: +1 (859) 323-1077, jsmalle@uky.edu.

are generally negative. For example, studies of the effects of titanium dioxide (TiO_2) nanoparticles on *Arabidopsis thaliana* have shown that particles of different size and surface characteristics can be internalized and can lead to extensive changes ranging from altered gene expression to proteasome inhibition and microtubule disassembly (Kurepa *et al.* 2010; Wang *et al.* 2011; Landa *et al.* 2012). The second best developed area of plant nanobiology is the bioproduction of nanoparticles using plants or plant extracts (Thakkar *et al.* 2010; Kharissova *et al.* 2013). The main question in this research area is how nanoparticles of some heavy metals (e.g., Ag, Cu, Au) are formed by exposing plants or plant extracts to aqueous metal salt solutions. Finally, the third and the least developed subarea in plant nanobiology explores the applied aspect of nanomaterial/plant interactions such as the development of tools for targeted herbicide, pesticide or fertilizer delivery (Torney *et al.* 2007; Gonzalez-Melendi *et al.* 2008; Perez-de-Luque and Rubiales 2009; Corredor *et al.* 2010; Rai and Ingle 2012).

In this current study, we focus on another applied aspect of plant nanobiology: the potential use of nanoparticles for the isolation of plant natural products. Titanium dioxide nanoparticles are among the best-studied nanomaterials (Arora *et al.* 2010). The large number of studies and the widespread use of TiO_2 nanoparticles in many areas of science and technology are a result of the unique properties of this nanomaterial that include photocatalytic ability, superconductivity and superhydrophylicity. TiO_2 in nature and at the nanoscale exists in three phases - anatase, rutile and brookite – which have different sizes of crystal cells and different electronic and optical properties (Mo and Ching 1995; Naicker *et al.* 2005). In addition to the physicochemical properties common to all TiO_2 phases, nanoscale anatase TiO_2 smaller than 20 nm has a specific surface reactivity. Molecules in the core of TiO_2 nanoparticles smaller than 20 nm have a regular anatase structure and are hexacoordinated. Surface molecules, on the other hand, are forced by confinement stress into a pentacoordinated, square pyramidal orientation. These anatase surface atoms bind atoms and molecules from the solution to compensate for the coordinative unsaturation. It has been shown that conjugation of TiO_2 nanoparticles with ortho-substituted bidentate ligands relaxes and heals the anatase surface with the highest efficiency (Rajh, Chen et al. 2002; Rabatic, Dimitrijevic et al. 2006). As a consequence, the stability of the chemical bonds formed on the TiO_2 nanoparicle surface precludes further modifications of surface atoms which may lead to reduced nanoparicle aggregation and decreased nonspecific interactions (Rajh *et al.* 2002; Thurn *et al.* 2009). This chemical property has been used to decorate TiO_2 nanoparticles with different functional ligands such as oligonucleotides, peptides, contrast agents and chemotherapeutic drugs (Paunesku *et al.* 2003; Paunesku *et al.* 2007; Arora *et al.* 2012), and it is essential for the method described in this study.

The flavonoids area large group of plant natural products that have a phenylbenzopyran structure (Marais *et al.* 2006). Flavonoids differ in the saturation of the pyran (C) ring, in the placement of the aromatic ring B at the positions C-2 or C-3 of ring C, and in the overall hydroxylation patterns. Flavonoids may be modified by hydroxylation, methoxylation, or *O*-glycosylation of hydroxyl groups as well as *C*-glycosylation directly to carbon atoms of the flavonoid skeleton (Marais *et al.* 2006). Of particular importance for this study is the fact that many flavonoids contain an enediol group, which suggest that they may act as bidentate ligands for anatase TiO_2 nanoparticles. If the chemical bond between flavonoids and TiO_2 nanoparticles is strong, desorbtion of the flavonoids from the anatase surface should be minimal, and thus the replacement of flavonoids with other bidentate ligands present in the vicinity of the nanoparticles (e.g., in a cellular milieu) is expected to be negligable. Therefore, anatase TiO_2 nanoparticles are predicted to be an efficient platform for the isolation of flavonoids.

The plant flavonoid biosynthetic pathway produces a great variety of pigmented and non-pigmented compounds (Grotewold 2006). Because large efforts have been devoted to cloning of the genes encoding the pathway enzymes and their transcriptional regulators, to the isolation of pathway mutants, and to the understanding of the environmental and endogenous regulation of the pathway, flavonoid biosynthesis is considered a model system for complex plant biosynthetic pathways (Grotewold 2006). Flavonoids are synthesized from the general phenylpropanoid pathway by the action of a metabolon associated with the cytoplasmic face of the endoplasmic reticulum, and after synthesis, they are transported to the vacuole where they accumulate (Marrs *et al.* 1995; Winkel-Shirley 2002; Winkel 2004). Some enzymes of the flavonoid pathway and some flavonoids have also been detected in the nucleus (Saslowsky *et al.* 2005; Polster *et al.* 2006). In addition, some aglicone flavonoids in Arabidopsis have been detected in membranes (Peer and Murphy 2006). The genes encoding flavonoid biosynthetic enzymes are under tight developmental, light, circadian and phytohormonal control, and are highly inducible by different adverse environmental signals (Winkel-Shirley 2002). Therefore, it is not surprising that flavonoid composition varies substantially during development and that it is influenced by growth conditions. Diverse methods for the analysis and identification of flavonoids have been established (Stobiecki and Kachlicki 2006). However, it needs to be noted that many of the naturally occurring flavonoid derivatives are labile, which tends to preclude their isolation and purification without degradation or chemical alteration (Stobiecki and Kachlicki 2006).

In this study, we used phosphorylated, ultra-small anatase TiO_2 nanoparticles to directly "harvest" flavonoids from Arabidopsis plants. We show that uptake of nanoparticles by intact plants or callus tissue leads to the formation of flavonoid-TiO_2 nanoconjugates that are spontaneously secreted into the incubation medium. As predicted by the specific surface chemistry of ultra-small anatase TiO_2 nanoparticles, mass spectrophotometric analyses of the isolated flavonoids revealed an enrichment of quercetin derivates that contain the catechol group. Thus, we introduce anatase TiO_2 nanoparticle-enabled nanoharvesting as a high-resolution, quantitative and scalable technique that allows the analyses of a specific fraction of the plant metabolome.

Results and discussion

Ultra-small anatase TiO_2 nanoparticles can bind Arabidopsis flavonoids *in vitro*

The ultra-small anatase TiO_2 nanoparticles, which we used for both *in vitro* and *in vivo* experiments, were first coated with phosphate ions by dialysis of bare nanoparticles against phosphate buffer. Phosphorylated TiO_2 nanoparticles are known to be more stable and to aggregate less at different pH values than bare nanoparticles (Wu *et al.* 2007), and thus offer a more stable functionalization platform for *in vivo* and *in vitro* experiments. Furthermore, phosphorylated TiO_2 nanoparticles were also shown to be more reactive towards enediol ligands (Wu *et al.* 2007).

Most Arabidopsis flavonoids are derivatives of the flavonols quercetin and kaempherol and the anthocyanidin species cyanidin (Veit and Pauli 1999; Yonekura-Sakakibara *et al.* 2008; Nakabayashi *et al.* 2009). To test if quercetin and kaempherol bind to ultra-small anatase TiO_2, we performed the *in vitro* surface functionalization of phosphorylated ultra-small anatase TiO_2 nanoparticles (Figure 1). We also tested *trans*-chalcone (1,3-diphenyl-2-propen-1-one), which has no enediol groups and is similar to the flavonoid biosynthesis intermediate chalcone (Figure 1a). Binding of functional groups to the nanoparticle surface can often be detected by (1) a color change of the nanoparticle suspension after addition of the functionalizing agent and (2) a shift in the absorption peaks of the functionalized nanoparticles (e.g., (Meng *et al.* 2008; Kurepa *et al.* 2010)). The UV-Vis absorption spectra of functionalized TiO_2 nanoparticles shows batochromic and/or hypochromic effects: the

maximal absorption peak of the functionalizing agent is red-shifted and broadened after it binds to nanoparticles. We observed a color change from yellow to orange when equimolar ratios of quercetin or kaempherol and ultra-small TiO_2 nanoparticles were mixed (Figure 1b). Comparison of the UV-Vis absorption spectra of the ultra-small TiO_2 nanoparticle suspension, quercetin or kaempherol solution, and quercetin- or kaempherol-TiO_2 nanoconjugate suspension proved that the nanoparticles have been functionalized: the prominent 375 nm quercetin and 370 nm kaempherol peaks were reduced in intensity and broadened towards the longer wave lengths. Thus, the UV-Vis absorption spectra of the nanoconjugates were characterized by both batochromic and hypochromic effects (Figure 1c). *trans*-Chalcone, on the other hand, did not alter the absorption of the TiO_2 nanoparticle suspension, suggesting that it did not bind to the nanoparticle surface (Figure 1).

Functionalization of TiO_2 nanoparticles with cyanidin and its glycosylated form cyanidin-3-glycoside has been studied with the aim to develop dye-sensitized solar cells (Cherepy *et al.* 1997; Meng *et al.* 2008). Cyanidin and its derivates have been shown to rapidly react with anatase nano-TiO_2 leading to the formation of the blue quinoidal cyanidin form from the red flavylium cyanidin form. To confirm that cyanidin-derived anthocyanins bind to our phosphorylated ultra-small anatase TiO_2 nanoparticles, we isolated total anthocyanins from aerial parts of four-week-old Arabidopsis plants, and added nanoparticles to the extracts. The color of the anthocyanin solution changed from pink to dark purple, suggesting the transition of cyanidin glycosides from the flavonium to the quinoidal form (Figure 2). The UV-Vis absorption spectra of the TiO_2 conjugates with anthocyanins showed hypochromic and batochromic effects. Different cyanidin derivates in Arabidopsis have a maximal absorption in the 518 nm–537 nm range (Shi and Xie 2010). In the anthocyanin-TiO_2 nanoconjugates sample, the cyanidin-specific absorption peak was broadened and red shifted to an apparent maximum of 590 nm. Thus, similar to purified cyanidin and cyanidin-3-glycoside (Cherepy *et al.* 1997; Meng *et al.* 2008), Arabidopsis cyanidin glycosides can form a stable complex with TiO_2 nanoparticles. In conclusion, phosphorylated ultra-small anatase TiO_2 nanoparticles can conjugate the major Arabidopsis flavonol aglicons as well as anthocyanins, which suggested that at least from the standpoint of their chemical reactivity, phosphorylated ultra-small anatase TiO_2 nanoparticles can be used for the isolation of flavonoids.

Anatase TiO_2 nanoparticles bind flavonoids *in planta*

The next essential requirement for the *in planta* conjugation of flavonoids to TiO_2 nanoparticles is that nanoparticles are imported into the plant cell and that they localize in the subcellular compartments that contain flavonoids. We have previously shown that ultra-small (3 – 5 nm) anatase TiO_2 nanoparticles are taken up by *Arabidopsis thaliana*, and are distributed in a tissue- and organ-specific manner (Kurepa *et al.* 2010). In many cell types (e.g., root cells and some epidermal cells), TiO_2 nanoparticles accumulated in the vacuole that is known to contain the largest cellular pool of flavonoids (Grotewold 2006; Kurepa *et al.* 2010). Since ultra-small anatase TiO_2 nanoparticles and flavonoids co-localize in the cell and because these nanoparticles can bind anthocyanin species and flavonol aglicones synthesized by Arabidopsis plants (Figures 1 and 2), we expected that flavonoid-TiO_2 nanoconjugates would form inside plant cells.

Compared to some other plant species, Arabidopsis plants are not a rich source of flavonoids. However, flavonoid metabolism in Arabidopsis is particularly well researched, and the identity of the flavonoid compounds has been determined and analyzed in different organs and at different stages of development (Veit and Pauli 1999; Yonekura-Sakakibara *et al.* 2008; Nakabayashi *et al.* 2009). It has been also established that the accumulation of anthocyanins in vegetative tissues is a hallmark of stress (Winkel-Shirley 2002; Lillo *et al.*

2008). To aid the visualization of nanoharvesting, we used both unstressed and stresses plants as the starting material. We selected a high-sucrose treatment to boost the anthocyanin content of Arabidopsis seedlings. The sucrose-dependent induction of genes involved in anthocyanin biosynthesis has been well documented (Tsukaya *et al.* 1991; Solfanelli *et al.* 2006; Lillo *et al.* 2008). The molecular mechanism responsible for the coordinative transcriptional regulation of anthocyanin biosynthetic genes has also been resolved, and it involves a sucrose-induced increase in the transcript level and presumably activity of the transcription factor PAP1 (Teng *et al.* 2005). In addition, the identities of the anthocyanin species that accumulate in sucrose-treated Arabidopsis plants have been described (Pourcel *et al.* 2009). Thus, currently the only unexplored effect of sucrose is the extent of the sucrose-induced changes in the flavonol metabolome.

We performed comparative mass spectrometric analyses of total flavonoids isolated from plants grown on normal and on high-sucrose medium (Figure 3 and Figure S2). In plants grown on high-sucrose medium, flavonol levels increased but the accumulation of all different flavonol species was not effected by sucrose to the same extent (Figure 3 and Figure S2). For example, analyses of the relative peak intensity of different flavonols in stressed versus unstressed plants revealed that extracts of plants grown on 4% sucrose were enriched in both quercetin and kaempherol derivates, but that different glycosides accumulated to different levels (Figure 3b, Figure S2 and Table S2; see Figure S1 nomenclature and structure of all Arabidopsis flavonoid species). The highest increase was observed for the most decorated flavonols f3 and f8 (3 and 6 times, respectively; Figure 3b and Table S2), whereas the increase of glucosylated forms f2 and f6 was not significant (Figure 3b and Table S2). The physiological relevance of the sucrose-induced flavonoid biosynthesis in general and the accumulation of highly glycosylated flavonoid species in particular is currently unknown. Nevertheless, the high-sucrose stressed Arabidopsis plants represented a complex pool of identified flavonoids which would be useful to follow and visualize nanoharvesting and determine the specificity of flavonoid binding to the TiO_2 nanoparticles.

To start testing if TiO_2 nanoparticles can also be coated with flavonoids via uptake in intact plant tissues, we co-incubated the nanoparticles with rosettes of plants grown for 4 weeks on media containing 1% or 4% sucrose (Figure 4a and Figure S3). After 4 hours of incubation in the dark at 22°C, a blue colored precipitate started to form around leaves of plants grown on 4% sucrose (Figure 4a and Figure S3). The blue color of these nanoconjugates suggested that TiO_2 induced the transition of cyanidin glycosides from the flavonium to quinoidal form, which occurs when cyanidin glycosides are bound to TiO_2 nanoparticles and exchange electrons. The precipitates were then pelleted, resuspended in phosphate buffer and used for spectrophotometric analyses. The UV-Vis spectra of the nanoconjugate suspensions isolated from plants grown on 1% or 4 % sucrose showed that nanoconjugates isolated from 4% sucrose-grown plants have two broad peaks: one with an apparent maximum at 600 nm, and the other at 400 nm. These two absorption maxima resemble the absorption peaks seen in the *in vitro* conjugation experiments with single flavonols and total anthocyanins, respectively (Figures 1 and 2). Co-incubation of other tissues (e.g., roots) with nanoparticles also resulted in the accumulation of TiO_2 nanoconjugates (Figure S3). Roots, which are known to have a different flavonoid composition compared to leaves (Yonekura-Sakakibara *et al.* 2008), yielded yellow-orange nanoconjugates (Figure S3). Thus, a simple co-incubation of plant tissues with ultra-small anatase TiO_2 nanoparticles led to the formation of extracellular nanoconjugates that have the expected spectral characteristics of TiO_2 nanoparticles functionalized with flavonoids.

Analyses of nanoharvesting parameters

Before engaging in the identification of molecules that are bound to anatase TiO_2 nanoparticles *in vivo*, we tested the effects of different parameters on the nanoharvesting yield. As expected, the quantity of flavonoids in plant tissues (e.g. total anthocyanin levels; Figure 4) and the concentration of nanoparticles used for the harvesting (Figure S4a,b) were positively correlated with the yield. Also as expected, the yield was influenced by the harvesting temperature: the lower the temperature, the lower the yield (Figure S4c). The effect of the pH of the co-incubation media was more complex. TiO_2 nanoparticle surface properties typically depend on the pH of the surrounding media: at low pH values, surface molecules become protonated (taking the form of TiO_2H_2) while at high pH values, they become hydroxylated. Because the net charge of anthocyanins is also pH-dependent, nanoharvesting was not effective at low and high pH (due to the mutual repulsion of nanoparticles and flavonoids) and has to be conducted at pH range of 5–7 (Figures S5 and S6).

Identification of flavonoids harvested by anatase TiO_2 nanoparticles

To determine the identities of the nanoharvested molecules, we released them from the nanoparticles at low pH and analyzed them using mass spectrometry (Figures 5, 6, S7 and Tables S1 and S2). These analyses revealed that both flavonol glycosides (kaempherol and quercetin derivates) and anthocyanins (cyanidin glycosides) were bound to the nanoparticles. Analyses of the relative abundances showed that, although almost all flavonoid species present in the plant cell bound to the nanoparticles, some molecules were isolated at disproportionately higher amounts. For example, comparison of different flavonols showed that quercetin derivates were enriched compared to kaempherol derivates in samples nanoharvested from both plants grown on 1% and 4% sucrose (Figure 5). In plants grown on 4% sucrose relative levels of quercetin derivates were 8.5 ± 2.5%, 7.6 ± 3.4% and 10.4% ± 2.9% for f3, f4 and f5, respectively. The relative levels of these compounds among the flavonols bound to anatase nanoparticles was 29.6 ± 14.6% (f3), 19 ± 8% (f4) and 32 ± 10.8 5 (f5) (Figure 5, Table S2). Thus, as predicted by the known surface reactivity of anatase nanoparticles, molecules with a catechol group (i.e., quercetin derivates) were enriched.

The f1 kaempherol derivate (kaempferol 3-O-α-L-rhamnopyranoside-7-O-α-L-rhamnopyranoside) was also nanoharvested with significant efficiency (Figure 5, Table S2). This kaempherol derivate is not more abundant than f2 and f3 (Figure 5, Table S2) which suggested that it is not the relative amount but rather a chemical property of f1 that led to its isolation by nanoharvesting. Since f1, f2 and f3 differ only in the sugar composition, it follows that sugar moieties function as a secondary “selection criteria” for binding to the nanoparticles. This was also the case for the anthocyanin species bound to anatase TiO_2 nanoparticles. All anthocyanin species in Arabidopsis are derivates of cyanidin that contains a catechol group in the ring B position. Comparison of the abundance of anthocyanin molecules present in the plant with those isolated by nanoharvesting showed that the “selection pressure” for binding to nanoparticles was driven by the nature of the sugar side-chains (Figure 6). For example, ~50% of the isolated anthocyanins are identified as the A3 derivate, which is one of the least abundant species in extracts of plants grown on 4% sucrose and is not detectable in plants grown on 1% sucrose (Figure 6, Tables S1 and S2). A1, A4, A6 and A7 derivates were also enriched. Structural analyses of the enriched anthocyanins revealed that the common characteristic is the presence of hydrogen in the R3 position (Figure 6). On the other hand, the presence of a synapoyl group in the R1 position acted as a “negative selection” for binding. The most striking example is A11, the most abundant cyanidin derivate in Arabidopsis. The relative abundance of A11 among the nanoharvested flavonoids was ~ 5% (Figure 6). Overall, these results suggested that the

flavonoids extracted by nanoharvesting were enriched for the presence of specific chemical groups, with the catechol group being the most favored.

The viability of plants and tissues after nanoharvesting

Exposure to nanoparticles results in a dose- and time-dependent decrease of cell viability (Manke *et al.* 2013; Suresh *et al.* 2013). The generation of reactive oxygen species (ROS) is the primary mechanism of nanoparticle toxicity (Nel *et al.* 2006). The capacity of nanoparticles to produce ROS inside the cell is influenced by their surface reactivity, chemical composition and interactions with cellular components (Nel *et al.* 2006). Thus, it is easily envisioned that co-incubation of plant tissues with ultra-small nanoparticles, which have a high surface-to-volume ratio, and therefore high surface reactivity, leads to cellular damage. Indeed, a 2-hour-long incubation with TiO_2 nanoparticles (76.6 mg/L) leads to a marked increase in superoxide radical production and in the number of cells stained with the SYTOX Green vital stain (Figure S8).

However, from the standpoint of the nanoharvesting methodology, some degree of cellular damage is inconsequential provided that it allows the source plant to survive the treatment. Thus, we next analyzed weather our nanoharvesting conditions allow the plants/tissues used as the source of flavonoids to remain viable and a continuous source for flavonoids of interest. For these assays, we used the *pap1-D* line which overexpresses the PAP1 MYB transcription factor (Borevitz *et al.* 2000) and thus has a high flavonoid content that allows the facile visualization of nanoharvesting. The use of the *pap1-D* line also circumvented the need for anthocyanin-inducing stress conditions, thus providing optimal growth conditions to test for viability and growth inhibition. We tested the post-harvesting viability in *pap1-D* seedlings and in calli from *pap1-D* hypocotyl explants (Figure 7). Both seedlings and calli were incubated for 4 hours at room temperature either in buffer or in the 76.7 mg/L suspension of anatase TiO_2 nanoparticles. Following the treatment, tissues were extensively washed in sterile water and used for viability tests. Treated calli were transferred to either calli or shoot inducing media (Figure 7a). After six weeks of incubation, calli incubated in buffer and in nanoparticles suspension did not differ either on calli-inducing or shoot-inducing media (Figure 7a). Similar to the *pap1-D* calli, seedlings treated with nanoparticles remained viable (Figure 7b). However, we observed that the root elongation of the treated seedlings was affected by the treatment (Figure 7b). Considering that nanoparticles preferentially bind to roots when whole seedlings are incubated in a nanoparticles suspension (Kurepa *et al.* 2010), it was not surprising that the root tissue was more affected by the treatment than the shoot.

The use of TiO_2 nanoparticles as a selective matrix to concentrate enediol compounds or to isolate and concentrate phosphorylated peptides has been reported previously (Pinkse *et al.* 2004; Larsen *et al.* 2005). However, both methods required the prior extraction of molecules of interest followed by post-treatment with nano-TiO_2. Our surprising finding that anatase nanoparticles can be used for the direct isolation of flavonoids from intact plant tissues implies that flavonoid-nanoparticle libraries can be easily prepared from limited amounts of tissues derived from different plants, organs or developmental stages. This isolation strategy could be particularly advantageous for the high-throughput, large-scale screening for novel secondary metabolites with therapeutic potential. In addition, anatase TiO_2 nanoparticles could be used not only as an isolation and enrichment matrix, but also as a delivery platform. Ultra-small 3–5 nm TiO_2 nanoparticles bound to different functional groups can enter metabolically active mammalian cells by endocytosis (Thurn *et al.* 2011). Thus, flavonoid/nanoparticle complexes prepared under sterile conditions in physiologically compatible buffers, could be used for treatments of mammalian cells in-line with the plant cell-based isolation step.

Furthermore, the flavonoid-nanoconjugates isolated from different sources could also serve as a selection platform for screens aimed at for example the identification of flavonoid-binding proteins. The inherent flexibility and scalability of nanoharvesting suggests it may be used as a versatile discovery tool. The uptake of TiO_2 nanoparticles by plants also suggests that this nanomaterial can be used for targeted delivery of compounds to plant cells. TiO_2 nanoparticles and TiO_2 nanocomposites have both been used for delivery of ligands to mammalian cells (Arora et al. 2012; Paunesku et al. 2003; Paunesku et al. 2007). In contrast to animals, methodology for delivery of different ligands (e.g., oligonucleotides, peptides or secondary metabolites) to plant cells and strategies for intracellular ligand release from TiO_2 nanoconjugates have not yet been developed.

Experimental Procedures

Nanomaterials

The synthesis and characterization of ultra-small anatase TiO_2 nanoparticles used in this study have been described (Kurepa *et al.* 2010). In brief, TiO_2 nanoparticles were synthesized by a low-temperature alkaline hydrolysis, dialyzed against sterile 10 mM Na_2HPO_4 pH 5.7 (Mini Dialysis Kit with a 1 kDa cut-off, GE Health Care, http://www3.gehealthcare.com), and either used immediately after dialyses or kept at 4 °C for a maximum of two weeks. Dialyzed nanoparticles aggregated, but were easily resuspended after vortexing and sonication for 5 minutes in the sonicating water bath. The average diameter of nanoparticles was 2.8 ± 1.4 nm and their characteristics have been previously described (Kurepa et al. 2010). Unless stated otherwise, the concentration of the TiO_2 nanoparticle suspension used was 76.67 mg/L and the total particle surface was 304 cm^2.

In vitro functionalization of TiO_2 nanoparticles

TiO_2 nanoparticle suspension (76.67 mg/L with surface site molarity of 4.11 mM) was mixed 1 volume of 4 mM quercetin, kaempherol or *trans*-chalcone dissolved in DMSO. Quercetin, kaempherol, and *trans*-chalcone were from Sigma-Aldrich (http://www.sigmaaldrich.com/). Surface functionalization was done for 30 minutes at 22°C. Prior to UV-Vis analyses, both nanoparticle and nanoconjugate suspensions were vortexed and sonicated for 1 min, and 1 μl was used to determine the absorption spectra using a NanoDrop 2000.

Plant lines and growth conditions

Two Arabidopsis lines were used: the wild-type Col-0 and *pap1-D*, a line overexpressing the PAP1 MYB transcription factor in the Col-0 background (Borevitz *et al.* 2000). Sterile-grown plants were used in all experiments. Seeds were surface sterilized (5 min 70% ethanol, 3 rinses with sterile water, 20 min 50% commercial bleach, and 3 rinses with sterile water) and stratified for 2 days. Plants were grown in a controlled environmental chamber (22°C, relative humidity ~60%, light of ~140 $\mu mols^{-1}m^{-2}$) on half-strength Murashige and Skoog medium (MS/2) at pH 5.7 (http://www.phytotechlab.com) containing 0.8% and either 1% or 4% sucrose.

Anthocyanin extraction for UV-Vis analyses

Prior to acidic aqueous methanol extraction (Kubasek *et al.* 1992), plants were blotted dry and weighed. Absorbance at 520 nm (peak absorption of cyanidin derivates) was measured using a DTX 880 Multimode Detector (Beckman Coulter).

Nanoharvesting

Sterile plants or dissected organs were immersed into a suspension of phosphorylated nanoparticles. The co-incubation was done on a rocker (10 rpm) at room temperature (22°C) in the dark. After harvesting, the plant tissue was removed, nanoparticles coated with metabolites were collected by centrifugation (1 min 1000 *g*), and the pellet was resuspended in 1/10 V of 10 mM Na phosphate buffer (pH 5.7). The suspension was used for UV-Vis analyses using a NanoDrop 2000.

Flavonoid-targeted analysis using LC-ESI-Q-TOF-MS

The areal parts of four-week-old plants were harvested, and separated in two batches. The first batch was lyophilized and used for the isolation of flavonoids as described (Yonekura-Sakakibara *et al.* 2008). In brief, lyophilized tissue was homogenized in MeOH-CH_3COOH-H_2O (9:1:10) using a mixer mill (MM 300, http://www.retsch.com/) with zirconia beads for 10 min at 20 Hz. The second batch was used for nanoharvesting. After nanoharvesting, plants were removed and nanoparticles were collected by centrifugation (1 min 1000 *g*). The bound molecules were released with MeOH-CH_3COOH-H_2O (9:1:10). After centrifugation at 15,000 *g* and filtration (Ultrafree-MC filter, 0.2 μm, Millipore), plant molecules released from nanoparticle surfaces (5 μl) were applied to an LC-MS system with an electrospray ionization (ESI) interface (LC, Waters Aquity UPLC system; MS, Waters Q-TOF Premier). The LC system conditions were: column, Aquity bridged ethyl hybrid (BEH) C18 (pore size, 1.7 μm, length 2.1 × 100 mm, Waters); column oven temperature, 38 °C; flow rate, 0.3 ml min^{-1}; solvent, solvent A (H_2O with 0.1 % formic acid) and solvent B (CH_3CN with 0.1 % formic acid); gradient profile, 0 min 10% B, 25 min 20% B, 27.5 min 100% B, 30 min 10% B. Lidocain was used as an internal standard. The MS conditions used were previously described (Matsuda *et al.* 2009).

Viability assays

To generate calli, *pap1-D* seeds were plated on MS/2 media, stratified for 2 days and exposed to light for 6 hours to promote germination. Seedlings were grown in the dark for 4 days and then transferred to light for an additional 7 days of growth to obtain long and thick hypocotyls. Hypocotyls were excised and positioned on MS media supplemented with 0.1 mg/L 2, 4-D and 0.25 mg/L kinetin to stimulate the generation of calli. After 6 weeks of cultivation, calli were excised, halved and one half was incubated in 10 mM sodium phosphate buffer pH 5.7 and the other in the nanoparticle suspension. Following the incubations, calli were extensively washed in sterile water and transferred to callus inducing plates (MS with 0.1 mg/L 2, 4-D and 0.25 mg/L kinetin and 2% sucrose) or shoot inducing plates (MS with 0.1 mg/L 2, 4-D and 0.6 mg/L 2-iP and 2% sucrose).

For seedling viability assays, *pap1-D* seedlings grown on vertically positioned MS/2 plates for six-days were incubated in buffer or in the nanoparticles suspension. After 4 hr, seedlings were removed from the harvesting solution, extensively washed in sterile water and returned to MS/2 plates. Initial root length was marked and plates were positioned vertically in the growth chamber. After 7 days of growth the root length was marked and the root length was calculated by subtracting the initial from the final length.

Supplementary Material

Refer to Web version on PubMed Central for supplementary material.

Acknowledgments

This work was funded by a grant from the Kentucky Tobacco Research and Development Center to J.S., and NIH grants R01EB002100 and U54 CA151880 to G.E.W.

References

Arora, H.; Doty, C.; Yuan, Y.; Boyle, J.; Petras, K.; Rabatic, B.; Paunesku, T.; Woloschak, G. Titanium dioxide nanocomposites. In: Challa, S.; Kumar, SR., editors. Nanomaterials for the Life Sciences Vol.8: Nanocomposites. Weinheim: WILEY-VCH Verlag GmbH & Co. KGaA; 2010. p. 1-42.

Arora HC, Jensen MP, Yuan Y, Wu A, Vogt S, Paunesku T, Woloschak GE. Nanocarriers enhance Doxorubicin uptake in drug-resistant ovarian cancer cells. Cancer Res. 2012; 72:769–778. [PubMed: 22158944]

Borevitz JO, Xia Y, Blount J, Dixon RA, Lamb C. Activation tagging identifies a conserved MYB regulator of phenylpropanoid biosynthesis. Plant Cell. 2000; 12:2383–2394. [PubMed: 11148285]

Cherepy NJ, Smestad JP, Grätzel M, Zhang JZ. Ultrafast electron injection: implications for a photoelectrochemical cell utilizing an anthocyanin dye-sensitized TiO_2 nanocrystalline electrode. J Phys Chem B. 1997:9342–9351.

Corredor E, Risueño MC, Testillano PS. Carbon-iron magnetic nanoparticles for agronomic use in plants: promising but still a long way to go. Plant Signal Behav. 2010; 5:1295–1297. [PubMed: 20930509]

Dietz KJ, Herth S. Plant nanotoxicology. Trends Plant Sci. 2011; 16:582–589. [PubMed: 21906987]

Gonzalez-Melendi P, Fernandez-Pacheco R, Coronado MJ, Corredor E, Testillano PS, Risueno MC, Marquina C, Ibarra MR, Rubiales D, Perez-De-Luque A. Nanoparticles as smart treatment-delivery systems in plants: Assessment of different techniques of microscopy for their visualization in plant tissues. Ann Bot. 2008; 101:187–195. [PubMed: 17998213]

Grotewold, E., editor. The Science of Flavonoids. New York: Springer Science; 2006.

Kharissova OV, Dias HV, Kharisov BI, Pérez BO, Pérez VM. The greener synthesis of nanoparticles. Trends Biotechnol. 2013; 31:240–248. [PubMed: 23434153]

Kubasek WL, Shirley BW, McKillop A, Goodman HM, Briggs W, Ausubel FM. Regulation of flavonoid biosynthetic genes in germinating *Arabidopsis* seedlings. Plant Cell. 1992; 4:1229–1236. [PubMed: 12297632]

Kurepa J, Paunesku T, Vogt S, Arora H, Rabatic BM, Lu J, Wanzer MB, Woloschak GE, Smalle JA. Uptake and distribution of ultrasmall anatase TiO_2 alizarin red S nanoconjugates in *Arabidopsis thaliana*. Nano Lett. 2010; 10:2296–2302. [PubMed: 20218662]

Landa P, Vankova R, Andrlova J, Hodek J, Marsik P, Storchova H, White JC, Vanek T. Nanoparticle-specific changes in *Arabidopsis thaliana* gene expression after exposure to ZnO, TiO2, and fullerene soot. J Hazard Mater. 2012; 241–242:55–62.

Larsen MR, Thingholm TE, Jensen ON, Roepstorff P, Jorgensen TJ. Highly selective enrichment of phosphorylated peptides from peptide mixtures using titanium dioxide microcolumns. Mol Cell Proteomics. 2005; 4:873–886. [PubMed: 15858219]

Lillo C, Lea US, Ruoff P. Nutrient depletion as a key factor for manipulating gene expression and product formation in different branches of the flavonoid pathway. Plant Cell Environ. 2008; 31:587–601. [PubMed: 18031469]

Ma X, Geiser-Lee J, Deng Y, Kolmakov A. Interactions between engineered nanoparticles (ENPs) and plants: Phytotoxicity, uptake and accumulation. Sci Total Environ. 2010; 408:3053–3061. [PubMed: 20435342]

Manke A, Wang L, Rojanasakul Y. Mechanisms of nanoparticle-induced oxidative stress and toxicity. Biomed Res Int. 2013; 2013:942916. [PubMed: 24027766]

Marais, JPJ.; Deavours, B.; Dixon, RA.; Ferreira, D. The Stereochemistry of flavonoids. In: Grotewold, E., editor. The Science of Flavonoids. New York: Springer Science; 2006. p. 1-47.

Marrs KA, Alfenito MR, Lloyd AM, Walbot V. A glutathione S-transferase involved in vacuolar transfer encoded by the maize gene *Bronze- 2*. Nature. 1995; 375:397–400. [PubMed: 7760932]

Matsuda F, Yonekura-Sakakibara K, Niida R, Kuromori T, Shinozaki K, Saito K. MS/MS spectral tag-based annotation of non-targeted profile of plant secondary metabolites. Plant J. 2009; 57:555–577. [PubMed: 18939963]

Meng S, Ren J, Kaxiras E. Natural dyes adsorbed on TiO_2 nanowire for photovoltaic applications: enhanced light absorption and ultrafast electron injection. Nano Lett. 2008; 8:3266–3272. [PubMed: 18788788]

Mo SD, Ching WY. Electronic and optical properties of three phases of titanium dioxide: Rutile, anatase, and brookite. Phys Rev B Condens Matter. 1995; 51:13023–13032. [PubMed: 9978097]

Monica RC, Cremonini R. Nanoparticles and higher plants. Caryologia. 2009; 62:161–165.

Naicker PK, Cummings PT, Zhang H, Banfield JF. Characterization of titanium dioxide nanoparticles using molecular dynamics simulations. J Phys Chem B. 2005; 109:15243–15249. [PubMed: 16852930]

Nakabayashi R, Kusano M, Kobayashi M, Tohge T, Yonekura-Sakakibara K, Kogure N, Yamazaki M, Kitajima M, Saito K, Takayama H. Metabolomics-oriented isolation and structure elucidation of 37 compounds including two anthocyanins from *Arabidopsis thaliana*. Phytochemistry. 2009; 70:1017–1029. [PubMed: 19497599]

Navarro E, Baun A, Behra R, Hartmann NB, Filser J, Miao A, Quigg A, Santschi PH, Sigg L. Environmental behavior and ecotoxicity of engineered nanoparticles to algae, plants, and fungi. Ecotoxicology. 2008; 17:372–386. [PubMed: 18461442]

Nel A, Xia T, Madler L, Li N. Toxic potential of materials at the nanolevel. Science. 2006; 311:622–627. [PubMed: 16456071]

Paunesku T, Rajh T, Wiederrecht G, Maser J, Vogt S, Stojicevic N, Protic M, Lai B, Oryhon J, Thurnauer M, Woloschak G. Biology of TiO_2-oligonucleotide nanocomposites. Nat Mater. 2003; 2:343–346. [PubMed: 12692534]

Paunesku T, Vogt S, Lai B, Maser J, Stojicevic N, Thurn KT, Osipo C, Liu H, Legnini D, Wang Z, Lee C, Woloschak GE. Intracellular distribution of TiO_2-DNA oligonucleotide nanoconjugates directed to nucleolus and mitochondria indicates sequence specificity. Nano Lett. 2007; 7:596–601. [PubMed: 17274661]

Peer, WA.; Murphy, AS. Flavonoids as signal molecules: Targets of flavonoid action. In: Grotewold, E., editor. The Science of Flavonoids. New York: Springer Science; 2006. p. 239-268.

Perez-de-Luque A, Rubiales D. Nanotechnology for parasitic plant control. Pest Manag Sci. 2009; 65:540–545. [PubMed: 19255973]

Pinkse MW, Uitto PM, Hilhorst MJ, Ooms B, Heck AJ. Selective isolation at the femtomole level of phosphopeptides from proteolytic digests using 2D-NanoLC-ESI-MS/MS and titanium oxide precolumns. Anal Chem. 2004; 76:3935–3943. [PubMed: 15253627]

Polster J, Dithmar H, Burgemeister R, Friedemann G, Feucht W. Flavonoids in plant nuclei: detection by laser microdissection and pressure catapulting (LMPC), in vivo staining, and UV-visible spectroscopic titration. Physiol Plantarum. 2006; 128:163–174.

Pourcel L, Irani NG, Lu Y, Riedl K, Schwartz S, Grotewold E. The formation of anthocyanic vacuolar inclusions in *Arabidopsis thaliana* and Implications for the sequestration of anthocyanin pigments. Mol Plant. 2009:1–13. [PubMed: 19529825]

Rai M, Ingle A. Role of nanotechnology in agriculture with special reference to management of insect pests. Appl Microbiol Biotechnol. 2012; 94:287–293. [PubMed: 22388570]

Rajh T, Chen LX, Lukas K, Liu T, Thurnauer M, Tiede DM. Surface restructuring of nanoparticles: an efficient route for ligand-metal oxide crosstalk. J Phys Chem B. 2002; 106:10543–10552.

Remédios C, Rosário F, Bastos V. Environmental nanoparticles interactions with plants: morphological, physiological, and genotoxic aspects. J Bot. 2012

Rico CM, Majumdar S, Duarte-Gardea M, Peralta-Videa JR, Gardea-Torresdey JL. Interaction of nanoparticles with edible plants and their possible implications in the food chain. J Agric Food Chem. 2011; 59:3485–3498. [PubMed: 21405020]

Saslowsky D, Warek U, Winkel B. Nuclear localization of flavonoid enzymes in Arabidopsis. J Biol Chem. 2005; 280:23735. [PubMed: 15817473]

Shi MZ, Xie DY. Features of anthocyanin biosynthesis in *pap1-D* and wild-type *Arabidopsis thaliana* plants grown in different light intensity and culture media conditions. Planta. 2010; 231:1385–1400. [PubMed: 20309578]

Solfanelli C, Poggi A, Loreti E, Alpi A, Perata P. Sucrose-specific induction of the anthocyanin biosynthetic pathway in Arabidopsis. Plant Physiol. 2006; 140:637–646. [PubMed: 16384906]

Stobiecki, M.; Kachlicki, P. Isolation and identification of flavonoids. In: Grotewold, E., editor. The Science of Flavonoids. New York: Springer Science; 2006. p. 47-70.

Suresh AK, Pelletier DA, Doktycz MJ. Relating nanomaterial properties and microbial toxicity. Nanoscale. 2013; 5:463–474. [PubMed: 23203029]

Teng S, Keurentjes J, Bentsink L, Koornneef M, Smeekens S. Sucrose-specific induction of anthocyanin biosynthesis in Arabidopsis requires the MYB75/PAP1 gene. Plant Physiol. 2005; 139:1840–1852. [PubMed: 16299184]

Thakkar KN, Mhatre SS, Parikh RY. Biological synthesis of metallic nanoparticles. Nanomedicine. 2010; 6:257–262. [PubMed: 19616126]

Thurn KT, Arora H, Paunesku T, Wu A, Brown EM, Doty C, Kremer J, Woloschak G. Endocytosis of titanium dioxide nanoparticles in prostate cancer PC-3M cells. Nanomedicine. 2011; 7:123–130. [PubMed: 20887814]

Thurn KT, Paunesku T, Wu AG, Brown EMB, Lai B, Vogt S, Maser J, Aslam M, Dravid V, Bergan R, Woloschak GE. Labeling TiO2 Nanoparticles with Dyes for Optical Fluorescence Microscopy and Determination of TiO2-DNA Nanoconjugate Stability. Small. 2009; 5:1318–1325. [PubMed: 19242946]

Torney F, Trewyn BG, Lin VS, Wang K. Mesoporous silica nanoparticles deliver DNA and chemicals into plants. Nat Nanotechnol. 2007; 2:295–300. [PubMed: 18654287]

Tsukaya H, Ohshima T, Naito S, Chino M, Komeda Y. Sugar-dependent expression of the *CHS-A* gene for chalcone synthase from petunia in trangenic Arabidopsis. Plant Physiol. 1991; 97:1414–1421. [PubMed: 16668565]

Veit M, Pauli GF. Major flavonoids from *Arabidopsis thaliana* leaves. J Nat Prod. 1999; 62:1301–1303. [PubMed: 10514319]

Wang S, Kurepa J, Smalle JA. Ultra-small TiO_2 nanoparticles disrupt microtubular networks in *Arabidopsis thaliana*. Plant Cell Environ. 2011; 34:811–820. [PubMed: 21276012]

Winkel BS. Metabolic channeling in plants. Annu Rev Plant Biol. 2004; 55:85–107. [PubMed: 15725058]

Winkel-Shirley B. Biosynthesis of flavonoids and effects of stress. Curr Opin Plant Biol. 2002; 5:218–223. [PubMed: 11960739]

Wu HP, Cheng TL, Tseng WL. Phosphate-modified TiO_2 nanoparticles for selective detection of dopamine, levodopa, adrenaline, and catechol based on fluorescence quenching. Langmuir. 2007; 223:7880–7885. [PubMed: 17564470]

Yonekura-Sakakibara K, Tohge T, Matsuda F, Nakabayashi R, Takayama H, Niida R, Watanabe-Takahashi A, Inoue E, Saito K. Comprehensive flavonol profiling and transcriptome coexpression analysis leading to decoding gene-metabolite correlations in *Arabidopsis*. Plant Cell. 2008; 20:2160–2176. [PubMed: 18757557]

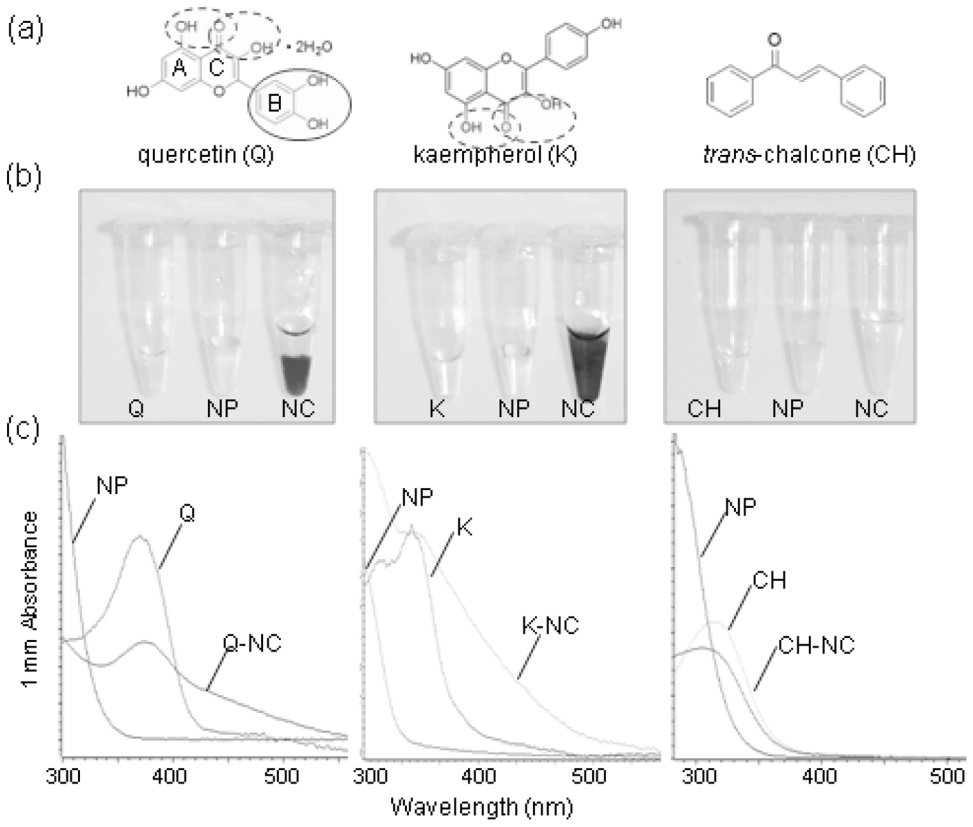

Figure 1. *In vitro* functionalization of phosphorylated TiO_2 nanoparticles (NP) with selected flavone aglicones

(a) Structure of quercetin (Q), kaempherol (K) and *trans*-chalcone (CH). The catechol group and vicinal hydroxyl groups that may bind to TiO_2 NPs are circled. The flavonoid rings A, B and C are labeled.

(b) Appearance of the TiO_2 NP suspensions after functionalization with Q, K or CH. Surface functionalization was carried out for 30 minutes at 22°C. thirty minutes-long functionalization at 22°C. Q-TiO_2 nanoconjugates (NC) mostly precipitated whereas K-TiO_2 NC remained in suspension.

(c) UV-Vis absorbance spectra of TiO_2 NP, Q, K, CH solutions and Q-, K- and CH-TiO_2-NC suspensions. Phosphorylated ultra-small anatase TiO_2 NPs do not absorb light at wavelengths above 350 nm. Compared to the Q and K solutions, the absorbance peak of Q- and K-coated TiO_2 NCs was broadened (hypochromic effect of the NP functionalization).

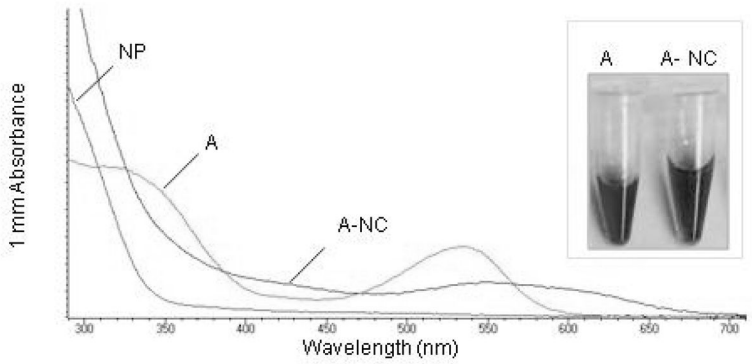

Figure 2. *In vitro* functionalization of phosphorylated ultra-small anatase TiO_2 nanoparticles (NP) with Arabidopsis anthocyanin (A) extract

Total anthocyanins were isolated using the acid methanol extraction method from four-week-old sterile-grown plants. NPs were added to the extract to final NP mass concentration of 76.7 mg/L and the suspension was incubated at 22°C for 30 minutes. UV-Vis spectra of anthocyanins and anthocyanin nanoconjugates (A-NC) shows that compared to the absorbance of the total anthocyanin extracts that has a prominent peak at 530 nm, the absorbance peak of A-NCs is red-shifted and broadened. Insert shows that the color off the anthocyanin solution changed from fuchsia to dark purple after the addition of TiO_2 NPs.

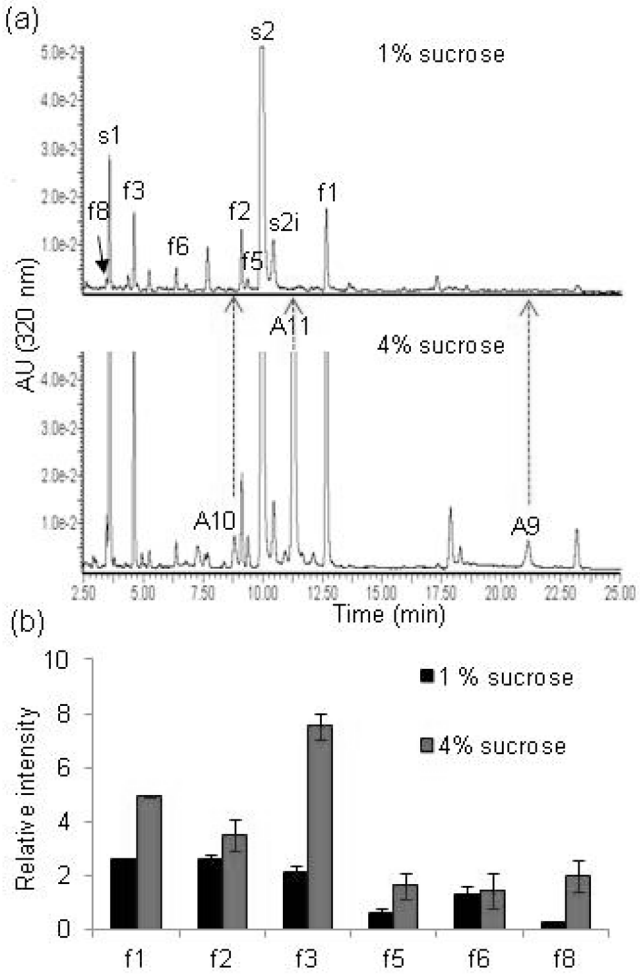

Figure 3. Analyses of sucrose-induced flavonols

(a) Representative UHPLC chromatograms of the aqueous acid methanol extracts from rosettes of four-week-old Col-0 plants grown on MS/2 media containing 1% or 4% sucrose. Labels correspond to compounds listed in Figure S1. s1, s2 and s2i are sinapoyl derivatives (Yonekura-Sakakibara et al., 2008). Detection: 320 nm.

(b) Relative levels of flavonol derivates in Col-0 plants grown on MS/2 media containing 1% or 4% sucrose. Relative abundance was calculated from average relative peak intensity and error bars are standard deviation. Source data are presented in Table S2.

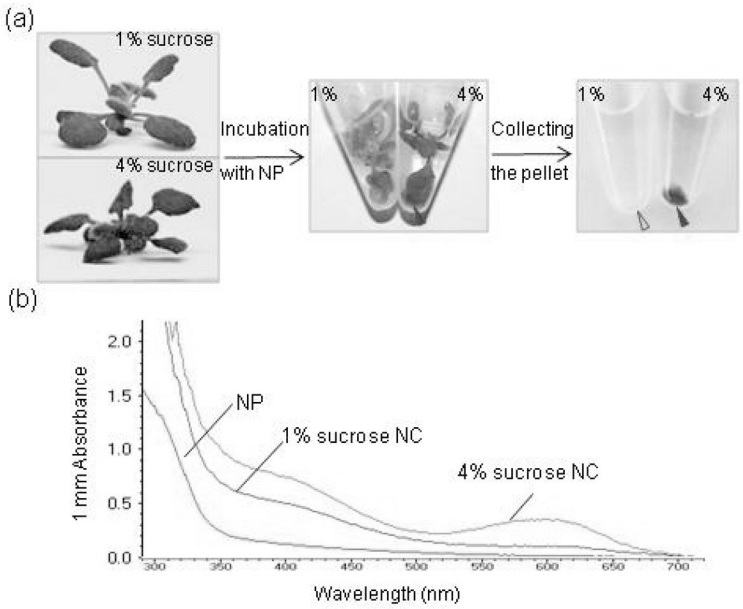

Figure 4. Nanoharvesting from Arabidopsis rosettes

(a) Nanoharvesting workflow. Four-week-old plants grown on MS/2 media with either 1% or 4 % sucrose were submerged into suspension of phosphorylated ultra-small anatase TiO_2 nanoparticles (NP) and incubated in the dark at 22°C for 2 hours. The final of the suspension was pH 6.0 and final mass concentration of nanoparticles was 76.7 mg/L. A blue precipitate (red arrow) formed around plants with high anthocyanin levels. The precipitate was pelleted by centrifugation.

(b) UV-Vis spectra of the nanoparticles used for harvesting, and the nanoconjugates (NC) isolated from plants grown on 1% or 4% sucrose. The nanoconjugate pellets shown in (a) were resuspended in 10 mM Na phosphate buffer, vortexed and sonicated prior to spectrophotometry.

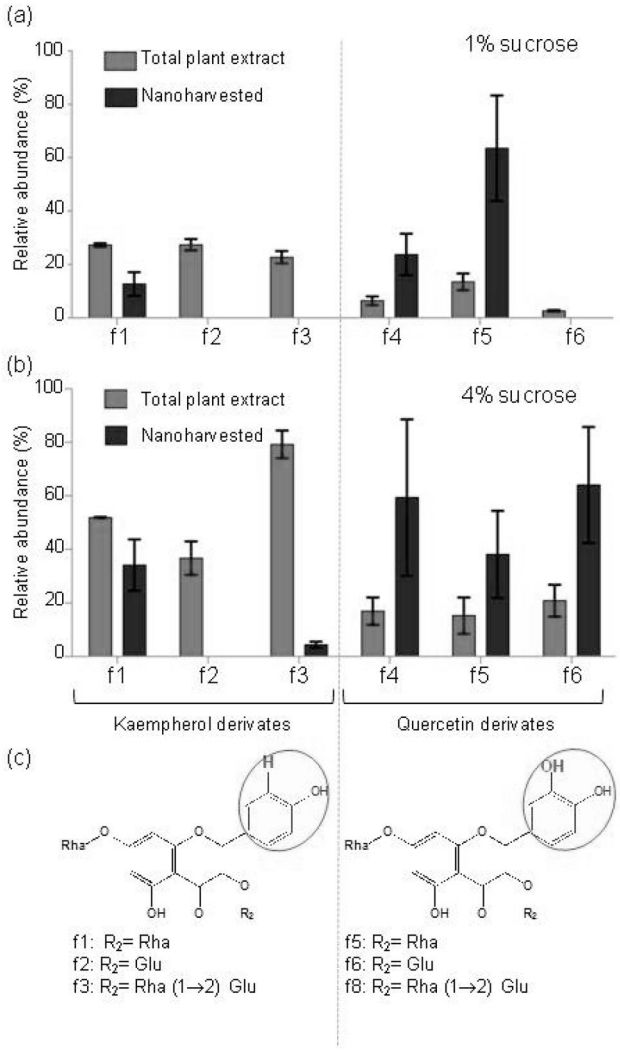

Figure 5. Selective nanoharvesting of flavonol derivates

(a) and (b) The relative abundance of flavonols in rosette extracts of plants grown on 1% (a) and 4% sucrose (b) media compared to relative abundance of flavonols released from nanoconjugates. The relative abundance was calculated from the average relative peak intensity (RI) ± relative standard deviation (RSD) (n=3). The sum of the relative peak of all detected flavonols was assigned the value of 100%.The source data are presented in Tables S1 and S2.

(c) Formulas of flavonol derivates detected in aqueous acid methanol extracts of plants and nanoconjugates. The phenol and catechol groups of the flavonol B ring are encircled, and the sugar moieties linked to the 3-*O* position of the flavonol ring (R2) are listed below the formulas. Rha, rhamnopyranose; Glu, glucopyranose.

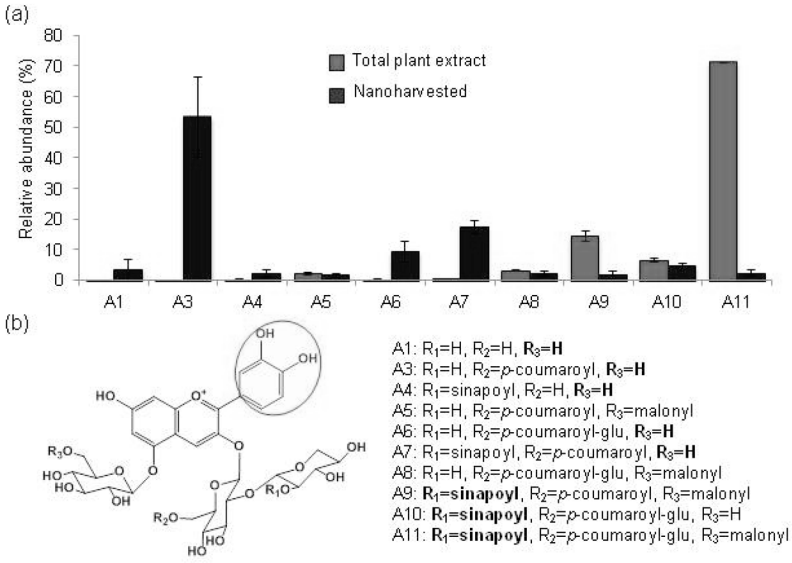

Figure 6. Selective nanoharvesting of cyanidin derivates from Col-0 plants grown on 4% sucrose

(a) The relative abundance of 3-*O*- and 5-*O*-sugar modified cyanidin derivates in rosette extracts compared to cyanidin derivates released from the nanoparticle coronas was calculated from the average relative peak intensity (RI) ± relative standard deviation (RSD) (n=3). The sum of the relative peak of all detected anthocyanin species was assigned the value of 100%.The source data are presented in Tables S1 and S2.

(b) Formulas of cyanidin derivates detected in aqueous acid methanol extracts of plants and nanoconjugates. The catechol group is encircled.

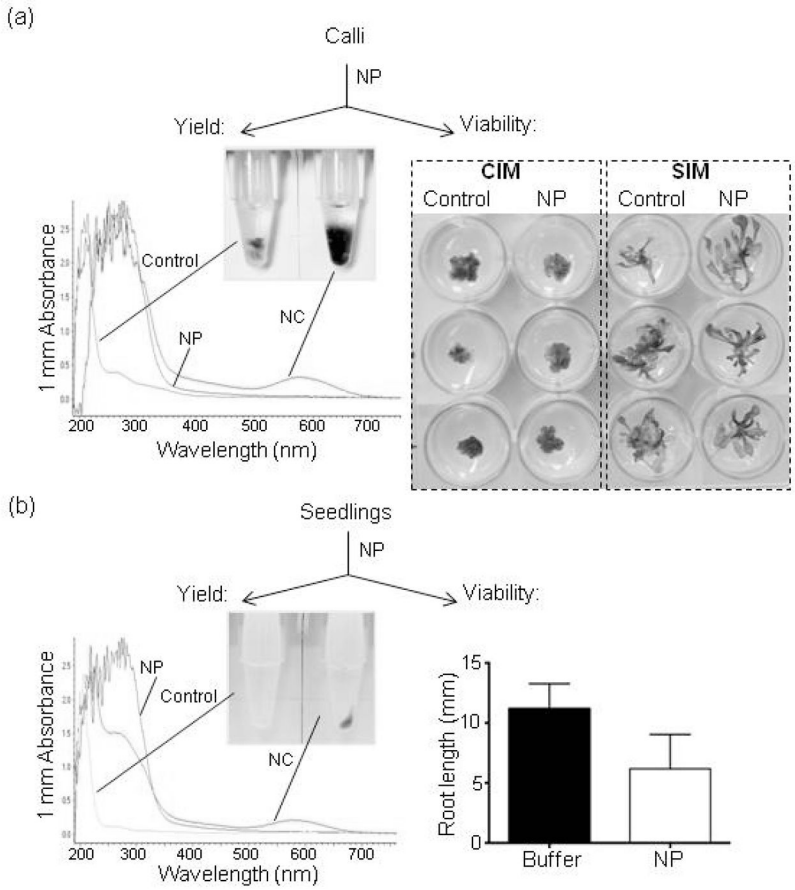

Figure 7. Post-harvesting viability of flavonoid source tissues

(a) Post-harvesting viability of calli. Calli from hypocotyl explants of *pap1-D* plants were incubated in 10 mM phosphate buffer or in 76.7 mg/L nanoparticle (NP) suspension. After a 4 hr treatment in the dark, calli were removed from the harvesting solution, washed in sterile water and transferred to callus induction media (CIM) or shoot induction media (SIM) to test viability. Calli and shoots were photographed 6 weeks after transfer. To determine nanoharvesting yield, the nanoconjugates (NC) suspension was vortexed, sonicated and 1 μl was analyzed by UV-Vis absorbance spectroscopy.

(b) Post-harvesting viability of seedlings. Seedlings were incubated in buffer or 76.7 mg/L nanoparticle suspension for 4 hr, then removed from the harvesting solution, extensively washed in sterile water and returned to MS/2 plates. Root elongation was measured after 7 days of growth on vertically positioned plates. Data are mean ± SD (n=10 seedlings per treatment, 2 replicate treatments). Harvested nanoconjugates were pelleted, resuspended in 50 μl of 10 mM phosphate buffer and 1 μl was analyzed by UV-Vis absorbance spectroscopy.